JCTC Journal of Chemical Theory and Computation

Article

pubs.acs.org/JCTC

Include Dispersion in Quantum Chemical Modeling of Enzymatic Reactions: The Case of Isoaspartyl Dipeptidase

Hai-Mei Zhang and Shi-Lu Chen*

Key Laboratory of Cluster Science of Ministry of Education, Beijing Key Laboratory of Photoelectronic/Electrophotonic Conversion Materials, School of Chemistry, Beijing Institute of Technology, Beijing 100081, China

Supporting Information

ABSTRACT: The lack of dispersion in the B3LYP functional has been proposed to be the main origin of big errors in quantum chemical modeling of a few enzymes and transition metal complexes. In this work, the essential dispersion effects that affect quantum chemical modeling are investigated. With binuclear zinc isoaspartyl dipeptidase (IAD) as an example, dispersion is included in the modeling of enzymatic reactions by two different procedures, i.e., (i) geometry optimizations followed by single-point calculations of dispersion (approach I) and (ii) the inclusion of dispersion throughout geometry optimization and energy evaluation (approach II). Based on a 169-atom chemical model, the calculations show a qualitative consistency between approaches I and II in energetics and most key geometries, demonstrating that both approaches are available with the latter preferential since both geometry and energy are dispersion-corrected in approach II. When a smaller model without Arg233 (147 atoms) was used, an inconsistency was observed, indicating that the missing dispersion interactions are essentially responsible for determining equilibrium geometries. Other technical issues and mechanistic characteristics of IAD are also discussed, in particular with respect to the effects of Arg233.

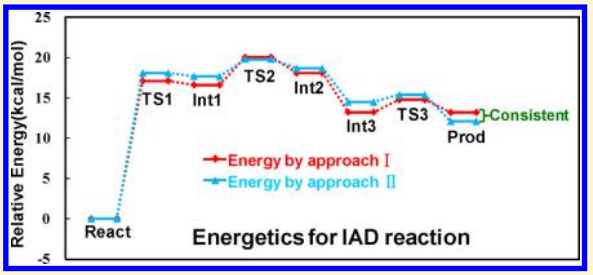

1. INTRODUCTION

In the past decade, quantum chemical modeling of enzyme active sites has proven to be a very fruitful approach to explore reaction mechanisms of enzymes and to provide insights into various aspects of catalysis.[1−7] There are many successful examples of enzymatic reaction mechanisms calculated using the density functional theory (DFT) methods,[1−28] in particular the B3LYP functional.[29−31] But for a few systems, the B3LYP method will cause relatively big errors. For example, the binding of methyl and adenosyl to cobalt in cobalamin-dependent enzymes have been reported to be greatly underestimated by 10−20 kcal/mol.[32] The energy differences between the peroxo and bis-μ-oxo isomers of copper dimer complexes also show large errors of 10−15 kcal/mol.[33,34] Recent studies indicate that the lack of dispersion in B3LYP is the main origin of this long-standing puzzling problem.[35,36] Geometry optimizations with B3LYP followed by single-point calculations of dispersion effects (using Grimme's empirical formula[37,38]) are able to correct these errors in dicopper complexes[35,39] and cobalamin-dependent enzymes.[35,36,40] Also, this approach (referred to as approach I in this work) has recently been successfully applied to a number of different systems, such as Ni-containing methyl-coenzyme M reductase,[41,42] heme-dependent chlorite dismutase,[43] photosystem II,[44] α-Keggin-type polyoxometalates,[45,46] and so on. With this, the essential dispersion effects in quantum chemical modeling of enzymatic reactions remain very attractive. How does dispersion affect quantum chemical modeling? How about the dispersion effects on geometries and energetics, respectively? How about the coupling effects of dispersion on both geometries and energies? Do the effects depend on the size of the chemical model? Is it necessary to involve dispersion also in the procedure of geometry optimization (unlike approach I mentioned earlier)? To explore the effects, it is necessary to perform an approach with dispersion included throughout geometry optimization and energy evaluation (here named by approach II). Approach I will also be employed in this work, because the use of approach I is able to provide completely "clean" dispersion corrections on the basis of nondispersion-corrected geometries (the dispersion effects can be separated for individual scrutiny), which renders it to be a useful reference method. The comparison between approaches I and II is capable of giving new insights into the effects of dispersion, thereby facilitating the development of quantum chemical methods used in mechanistic studies of enzymes and also metal-containing complexes. Since a number of investigations[35,36,39−46] have been done using approach I (as described earlier), the studies in this work are also able to check the validity of previous works by approach I.

Considering the purpose of this work, we chose an enzyme with a generally well-formulated mechanism, that is, isoaspartyl dipeptidase (IAD). It is a binuclear zinc enzyme that catalyzes the hydrolysis of β-aspartyl dipeptides, which contain a peptide

Received: March 15, 2015
Published: May 7, 2015

DOI: 10.1021/acs.jctc.5b00246
J. Chem. Theory Comput. 2015, 11, 2525−2535

bond to the β-carboxylate group of aspartic acid.[47] The overall reaction catalyzed by IAD is presented in Scheme 1.

Scheme 1. Hydrolysis of β-Aspartyl Dipeptide Catalyzed by Isoaspartyl Dipeptidase (IAD)

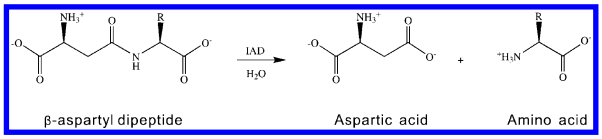

Several X-ray crystal structures of IAD have been determined, including the free enzyme (PDB code: 1ONW)[48] and IAD (or IAD mutant) with inhibitors bound (1ONX[48] and 1YBQ[49]). The crystal structure of free enzyme (1ONW) shows that IAD is a homodimeric metalloenzyme containing two zinc ions in each active site (see Figure 1). The

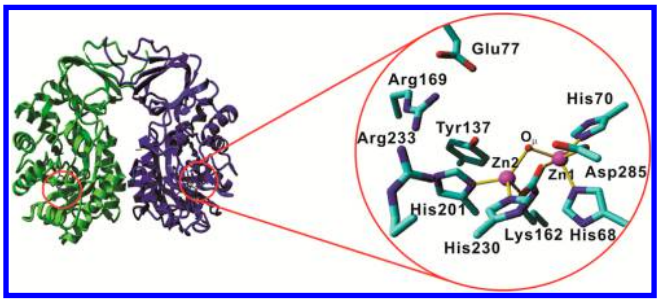

Figure 1. Overall structure of wild-type IAD and close-up view of the active site. Coordinates from PDB entry 1ONW[48] were used to generate the pictures.

two zinc ions (Zn1 and Zn2) are separated by ~3.4 Å and bridged by a carboxylated Lys162 and an oxygen species (Figure 1). The latter bridging species has been proposed to be a hydroxide ($O_\mu H^-$)[50] and function as an initial neucleophile during the catalysis (discussed later).[49] The Asp285 is hydrogen bonding to the bridging hydroxide. This residue (Asp285) was suggested to act as a special deliverer to transport the proton of $O_\mu H^-$ (H_μ) to the nitrogen of the substrate peptide bond (N_S) in the reaction.[49] Another crystal structure of the IAD mutant D285N complexed with β-aspartyl histidine (1YBQ)[49] gives a clear indication to substrate binding: the substrate is located in the active-site pocket via a few hydrogen bonds to several second-shell residues including Arg169, Arg233, Glu77, and Tyr137, with the oxygen (O_S) and carbon (C_S) of the substrate peptide bond orientated toward the Zn2 and O_μ atoms, respectively.

On the basis of crystal structures and various catalytic properties of the mutant and wild-type enzymes, a reaction mechanism for the IAD-catalyzed hydrolysis of β-aspartyl dipeptides has been formulated (Scheme 2).[49] With the substrate docking onto the active site, the bridging hydroxide ($O_\mu H^-$) performs a nucleophilic attack at the carbonyl carbon of the substrate peptide bond (C_S), simultaneously with a proton transfer from the hydroxide to the carboxylate of Asp285. This step leads to a tetrahedral *gem*-diolate intermediate, which may be stabilized by the Zn2 cation. Next, another proton transfer takes place from Asp285 to the nitrogen of the substrate peptide bond (N_S) concomitant with the C_S–N_S bond cleavage, resulting in two amino acid products. To complete the catalytic cycle, the active site should be regenerated, involving the product leaving and the

Scheme 2. Proposed Reaction Mechanism of IAD

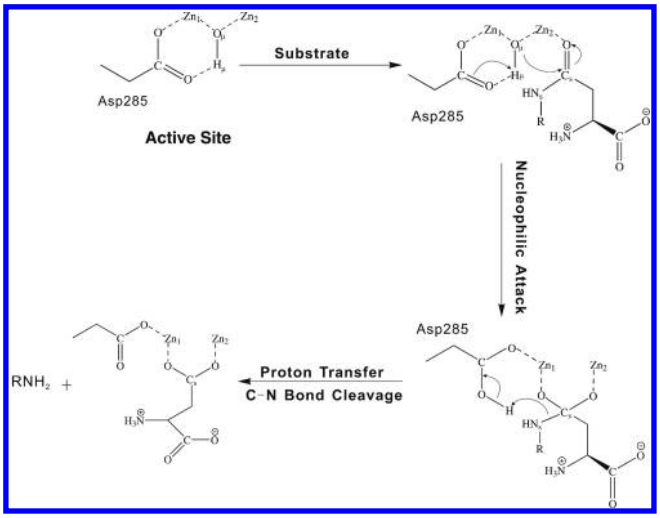

rebridging between the two zinc ions by a hydroxide derived from a water molecule. However, exactly how the regeneration happens is still unclear. Therefore, the regeneration process of the IAD active site will not be calculated in this work.

In the present work, with IAD as an example, we have made the comparison between approaches I and II and provide the discussion of some technical issues involved. Using approaches I and II respectively, we have calculated the potential energy profile for the IAD reaction and present the characterization of stationary points. The calculations show that approaches I and II can give qualitatively consistent results and lead to the same conclusions about the IAD reaction mechanism when a 169-atom chemical model is used, demonstrating that both approaches are available and effective for the modeling of enzymatic reactions, but with approach II preferential since both geometry and energy are dispersion-corrected in that. However, with a smaller model used (without Arg233), an inconsistency between approaches I and II was observed. This implies that the dispersion interactions missing with the removal of Arg233 are essentially responsible for determining equilibrium geometries.

2. COMPUTATIONAL METHODS

All calculations were performed using the DFT functional B3LYP,[29−31] as implemented in the Gaussian 09 D01 program package.[51] Geometry optimizations were carried out with the 6-31G(d, p) basis set for all atoms except Zn, for which the LANL2DZ basis set was used. Based on the optimized geometries, more accurate energies were obtained by performing single-point calculations with a larger basis set 6-311+G(2d,2p) for all elements. Solvation effects were calculated at the same theory level as the optimizations by performing single-point calculations on the optimized structures using the conductor-like polarizable continuum model (CPCM) method.[52−55] The dielectric constant (ε) was chosen to be 4, which is a standard value used in these kinds of applications.[56] A systematic benchmark of CPCM has been made by Yu and Houk.[57] Frequency calculations were performed at the same theory level as the optimizations to obtain zero-point energies (ZPE) and to confirm the nature of stationary points. Dispersion corrections were calculated using the empirical formula by Grimme et al. (i.e., DFT-D3).[37,38,58,59] It is worth stressing again that approach I named here includes

DOI: 10.1021/acs.jctc.5b00246
J. Chem. Theory Comput. 2015, 11, 2525−2535

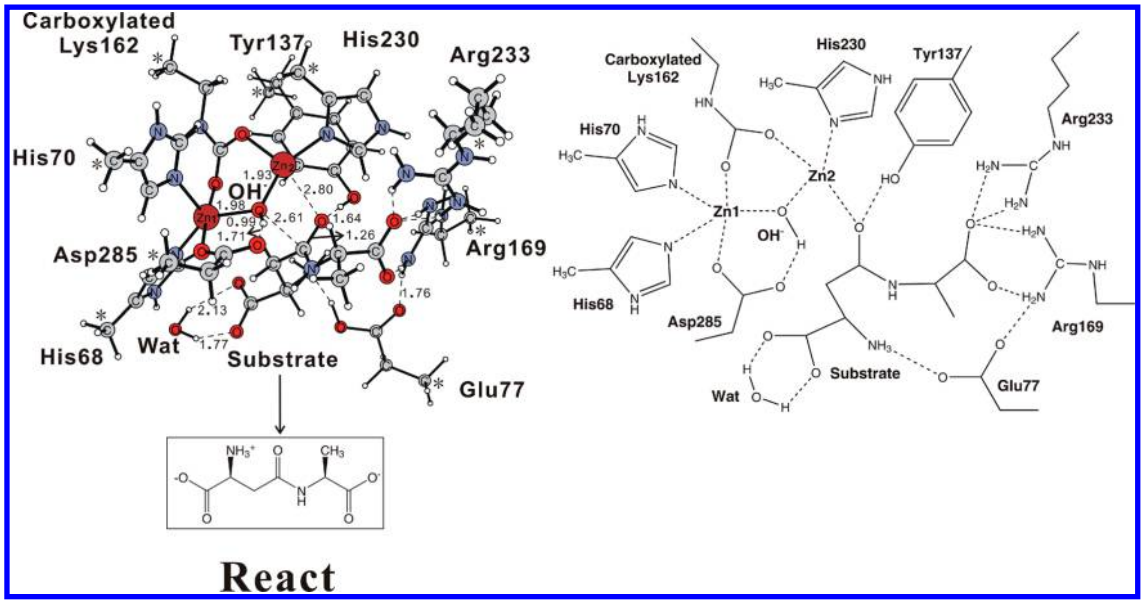

Figure 2. Optimized structure of the IAD active site with a β-aspartyl alanine bound (left) and its schematic structure (right). For clarity, His201 (a Zn2 ligand) is omitted. Asterisks indicate the atoms that are fixed to their X-ray positions. Inserted is the model substrate used in calculations. Wat: a water molecule. All distances are in angstroms.

dispersion only in energy corrections via single-point calculations, while approach II contains dispersion in both geometry optimization and energy evaluation. If not otherwise indicated, the energies reported in this work are corrected for ZPE, solvation effects, and dispersion effects. In addition, Cartesian coordinates of optimized structures with and without dispersion included are given in the Supporting Information (SI).

The present procedure, termed cluster modeling, has been successfully used to study a large number of enzyme mechanisms in the past decade. A comprehensive review has recently been written.[1] It is worth noting that in many cases the use of one method with a reasonable accuracy is a better choice than this kind of mixing of different methods (especially the mixing of basis sets). In the calculations of uncatalyzed hydrolysis of β-aspartyl alanine (discussed later), the larger basis set 6-311+G(2d,2p), solvation, and dispersion effects are used throughout the geometry optimizations and frequency calculations. The employment of this mixing in the present work is mainly due to the balance between accuracy and efficiency, because the use of a higher level method is very expensive for such a large system. Fortunately, this kind of cluster modeling has been shown to be quite sound by careful benchmarks.[1,3,28,60] In particular, it has been found that geometry optimization is not sensitive to the size of the basis set but energy is when the B3LYP functional is used in the modeling. Therefore, in this work, we will not discuss the routine procedure of cluster modeling any further but rather focus on the inclusion of dispersion. The B3LYP-D3 method used in this work is a very cheap (hardly having extra consumption) update way which is easily applied on top of the previous results of the well-established B3LYP. There is also a good collection of functionals suited for calculations of reaction energy profiles,[61] e.g., PBE0[62−64] and BB1K,[65−67] but they will not be discussed here.

3. RESULTS AND DISCUSSION

3.1. Chemical Model. A model of the IAD active site (Figure 2) was constructed on the basis of a crystal structure of wild-type IAD complexed with a β-aspartate product (PDB entry 1ONX).[48] In this case, it is expected that the use of a crystal structure with a product inhibitor bound may provide an initial geometry as close as the enzyme−substrate complex. The model contains the two zinc ions along with their bridging species (carboxylated Lys162 and hydroxide, $O_\mu H^-$) and ligands (His68, His70, His230, His201, and Asp285). In principle it is possible to clarify whether the oxygen bridging species is a hydroxide or a water molecule by quantum chemical investigations. The calculations of each reaction pathway with hydroxide or water and the subsequent comparison of energy barriers are able to determine the oxygen species. In this study, a hydroxide ($O_\mu H^-$) was employed in the model since it has previously suggested to be the bridging species.[50] As mentioned earlier, several second-shell residues (Arg169, Arg233, Glu77, and Tyr 137) play the role in assisting in substrate binding. Thus, they are also included in this model. To reduce the size, some truncations of residues have been made. To preserve the spatial arrangement of the residues, the atoms where the truncations have been made were fixed to their X-ray crystal positions. These centers are indicated by asterisks in later figures. β-Aspartyl alanine, a β-dipeptide, was chosen as the model substrate in the present study. It should be mentioned that all carboxylate groups in the model are charged by −1, while the amido in the β-aspartyl moiety of the substrate is presented as $-NH_3^+$. The substrate was placed in the active site according to the binding indication by the crystal structure of IAD mutant D285N complexed with β-aspartyl histidine (1YBQ).[49] The exposed carboxylate in β-aspartyl moiety is solvated by a water molecule (indicated by Wat in Figure 2). With the model substrate as well as the additional water bound, the total number of atoms in the model is 169 and the total charge is +1.

The optimized structure of the IAD active site with the model substrate bound, referred to as React, is displayed in

DOI: 10.1021/acs.jctc.5b00246
J. Chem. Theory Comput. 2015, 11, 2525−2535

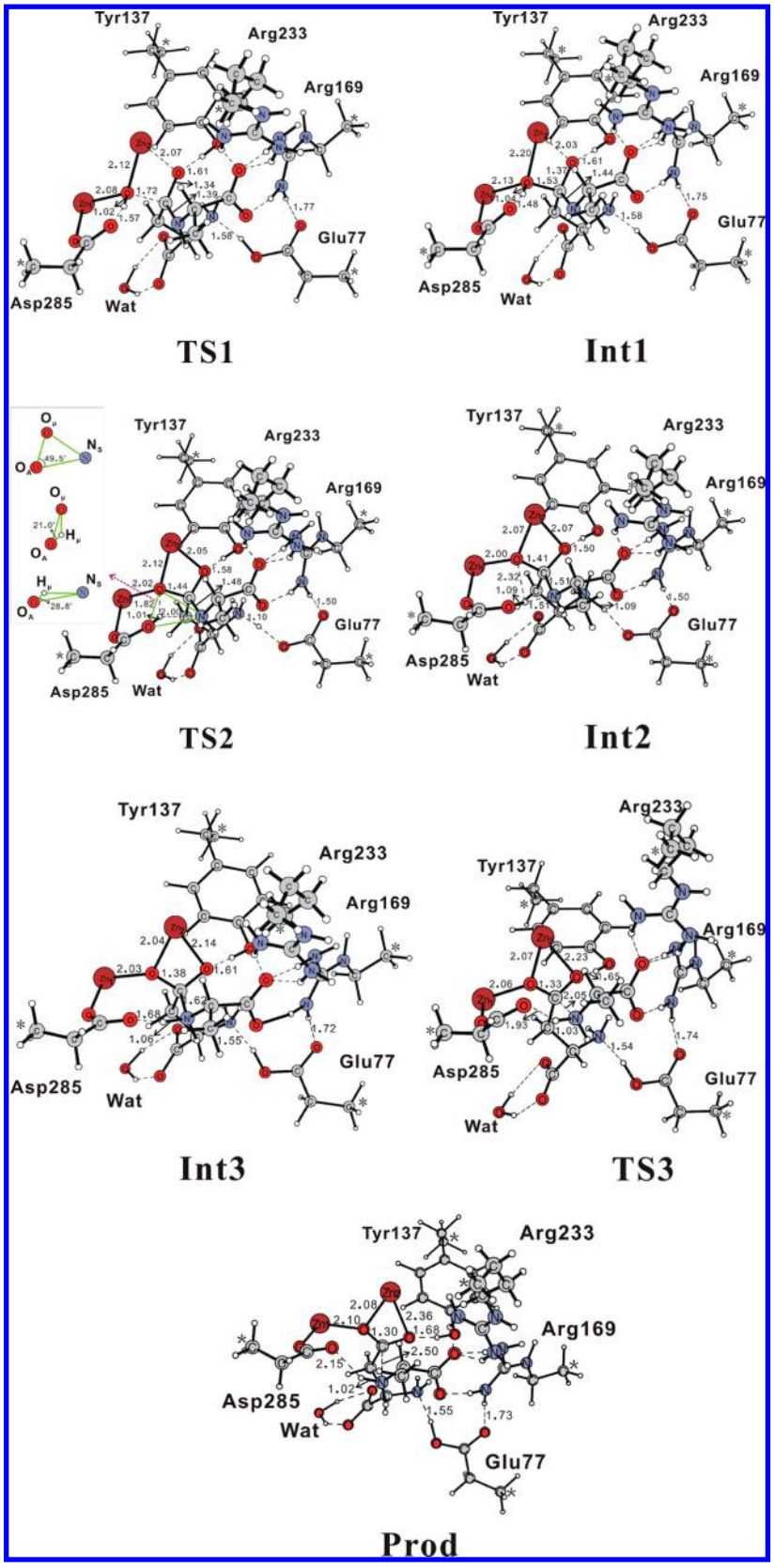

Figure 3. Optimized structures of stationary points along the reaction pathway calculated by approach II. For clarity, a few ligands are omitted, including His70, His68, His230, His201, and carboxylated Lys162, which is also applied to Figure 5.

Figure 2. The overall geometric parameters obtained from the geometry optimization agree well with the X-ray structure. For example, the computed Zn1−Zn2 distance (3.39 Å) is in excellent agreement with the crystallographic distance of 3.38 Å in the wild-type free enzyme (1ONW).[48] The substrate of β-aspartyl alanine is bound in the active site via several hydrogen

DOI: 10.1021/acs.jctc.5b00246
J. Chem. Theory Comput. 2015, 11, 2525−2535

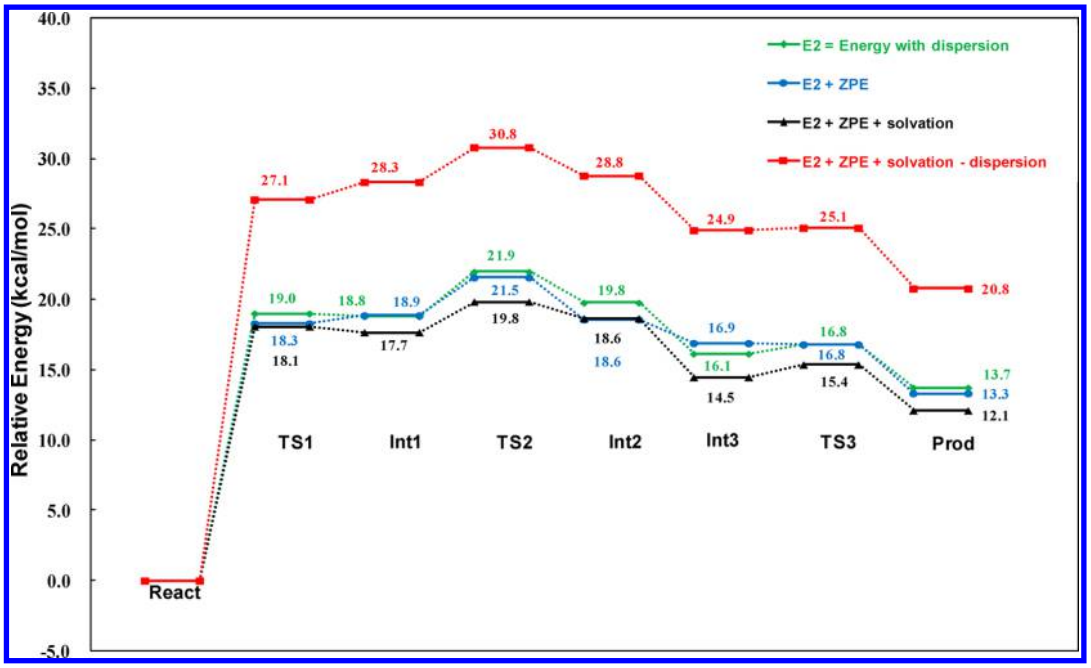

Figure 4. Potential energy profile for the IAD reaction calculated by approach II. E2: B3LYP/6-311+G(2d,2p) energies obtained by approach II. ZPE: Zero-point energies. Solvation: CPCM solvation effects added with dielectric constant $\varepsilon = 4$.

bonds to the second-shell residues, with the carbonyl carbon of the peptide bond (C_S) located at a distance of 2.61 Å to the O_μ atom, a reasonable distance for the initial step of nucleophilic attack.

3.2. Mechanism Calculated by Approach II. *3.2.1. Nucleophilic Attack.* It has been proposed that, once the substrate is bound, the bridging hydroxide will perform a nucleophilic attack on the carbonyl carbon of the peptide bond (C_S).[49] From the enzyme−substrate complex (React), a transition state for this reaction step (TS1) and the resultant intermediate (Int1) have been optimized and displayed in Figure 3. The TS1 has been confirmed to be a first-order saddle point with an imaginary frequency of 300*i* cm^{-1}. At TS1, the key O_μ−C_S distance is calculated to be 1.72 Å, which is shortened to 1.53 Å at Int1. With the O_μ−C_S bond formed at Int1, the peptide carbonyl double bond is elongated to 1.37 Å from 1.26 Å at React (via 1.34 Å at TS1), indicating that a tetrahedral *gem*-diolate intermediate is generated and negative charge is developed at the carbonyl oxygen (O_S). The Mulliken charge at the O_S atom is increased to −0.77 at Int1 from −0.58 at React (via −0.74 at TS1). The developing charge at the O_S atom leads to its coordination to the Zn2 ion (2.07 Å at TS1 and 2.03 Å at Int1). This demonstrates that Zn2 provides catalytic power by stabilizing the developing negative charge of the O_S atom. In the Int1 intermediate, the O_μ atom still keeps bridging to Zn1 and Zn2 with the distances of 2.13 and 2.20 Å, respectively. The distance of the $O_\mu H^-$ hydrogen (H_μ) to one of Asp285 oxygens (O_A) is shortened to 1.48 Å from 1.71 Å at React (via 1.57 Å at TS1).

The barrier for this step of nucleophilic attack is calculated to be the feasible 19.0 kcal/mol in the cluster model (18.3 kcal/mol with ZPE) (see Figure 4). Upon the addition of surrounding solvation in the form of CPCM,[52−55] the barrier slightly decreases to 18.1 kcal/mol. A table including ZPE, solvation, and dispersion corrections is also given in the SI (Table S1). The Int1 intermediate is calculated to be 18.8 kcal/mol higher than the reactant (18.9 kcal/mol with ZPE, 17.7 kcal/mol including ZPE and solvation). It is worth noting that, with the addition of ZPEs to the cluster-model energies (i.e., E2 in Figure 4), Int1 (18.9 kcal/mol) becomes slightly higher than TS1 (18.3 kcal/mol) in energy. This is an error originated from the incorporation of the ZPEs obtained with a medium-size basis set into the energies calculated with a larger basis set. Although these types of errors appear several times in the present work and other studies,[68,69] they should not alter any conclusions about the mechanism since they are very small. For example, in this case of IAD the ZPE corrections are usually smaller than 1 kcal/mol (see Figure S1 in the SI) and are thus unimportant. It should also be pointed out that the cluster-model energies mentioned earlier (the green curve in Figure 4) already contain dispersion corrections, since dispersion effects are included in both geometry optimization and energy evaluation in approach II. Based on the geometries of Figures 2 and 3, the single-point calculations without dispersion corrections were performed to give the energies without approach II-derived dispersion (see the red curve in Figure 4). A comparison between the black and red curves in Figure 4 can offer the dispersion effects in every chemical step. It can be seen that the dispersion corrections for the reaction barrier (−9.0 kcal/mol) and energy (−10.6 kcal/mol) are not small in the first step of nucleophilic attack. This can be rationalized by considering that this step involves the substrate approaching the dizinc core in a relatively long distance. For example, the distances of the substrate carbonyl oxygen (O_S) and carbon (C_S) to the Zn2 and O_μ atoms are significantly shortened from 2.80 and 2.61 Å at the reactant state (React of Figure 2) to 2.03 and 1.53 Å at the intermediate (Int1 of Figure 3), respectively. It is worth noting that the O_S−Zn2 and C_S−O_μ distances are kept approximately the same in the following steps, which results in very small dispersion effects for the stationary points after Int1 (discussed later).

3.2.2. Proton Transfer. It has been suggested that,[49] from the tetrahedral *gem*-diolate intermediate (Int1), the H_μ proton has to be transferred from $O_\mu H^-$ to the nitrogen of the peptide

DOI: 10.1021/acs.jctc.5b00246
J. Chem. Theory Comput. 2015, 11, 2525−2535

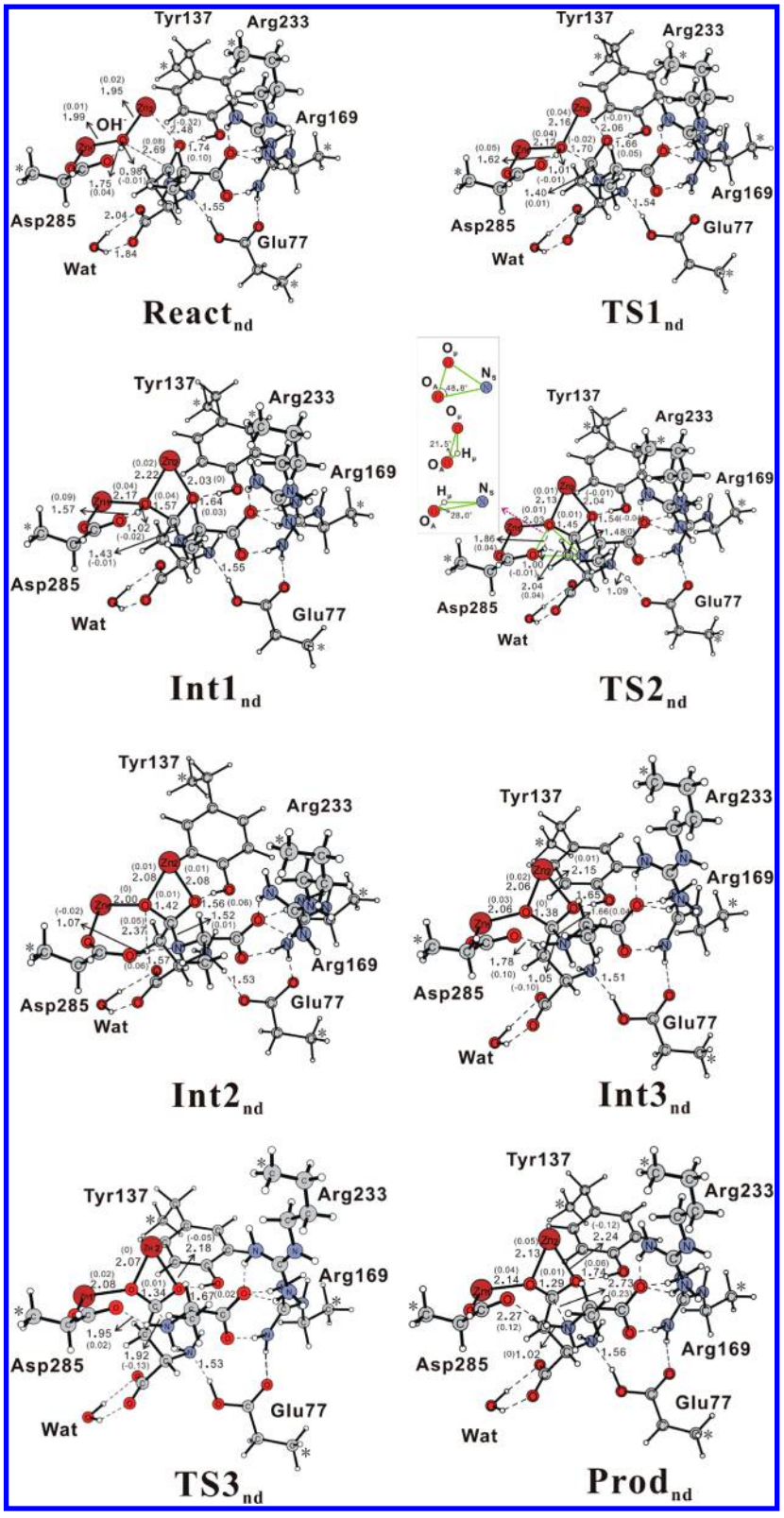

Figure 5. Optimized structures of stationary points along the reaction pathway calculated by approach I. Key distance differences between this figure and Figure 3 of the corresponding stationary points are shown in parentheses.

bond (N_S) with the help of Asp285, before the C_S–N_S peptide bond can cleave. Our calculations described later demonstrate that this process is most likely achieved through two steps, i.e., a proton transfer from $O_\mu H^-$ to the oxygen of Asp285 (O_A) followed by another proton transfer from O_A to N_S.

A transition state (TS2, Figure 3) for the proton transfer from $O_\mu H^-$ to O_A was obtained and its nature was confirmed by a frequency calculation to have an imaginary frequency of 276*i* cm^{-1}. It is very interesting to find that, simultaneously with the proton transfer, the resulting O_AH group rotates toward the

DOI: 10.1021/acs.jctc.5b00246
J. Chem. Theory Comput. 2015, 11, 2525−2535

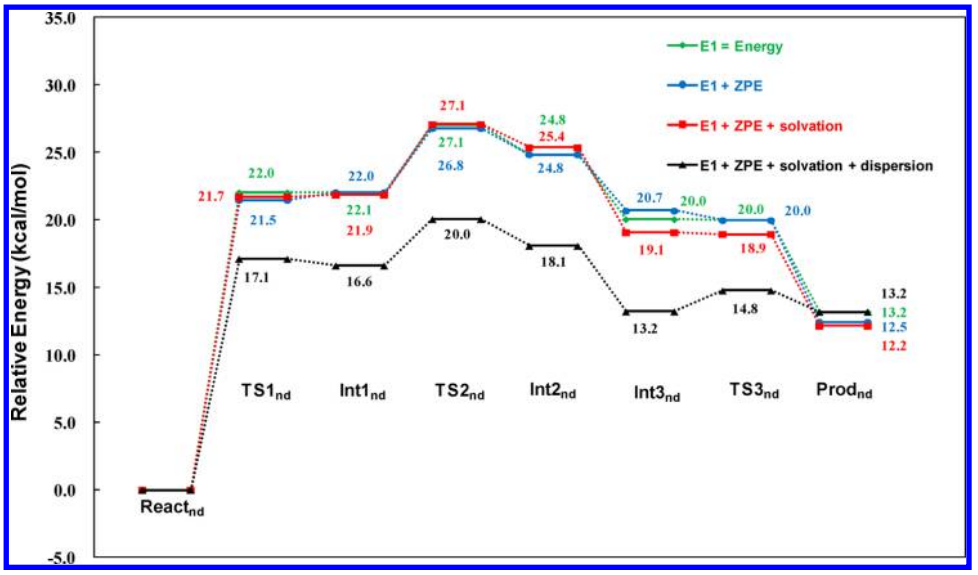

Figure 6. Potential energy profile for the IAD reaction calculated by approach I. E1: B3LYP/6-311+G(2d,2p) energies obtained by approach I. ZPE: Zero-point energies. Solvation: CPCM solvation effects added with dielectric constant $\varepsilon = 4$. Dispersion: Dispersion corrections obtained by single-point DFT-D3 calculations.

N_S atom leading to an intermediate (Int2, Figure 3) with a new hydrogen bond between them. At TS2, the O_AH group is located inside the angle of $\angle O_\mu O_A N_S$ (49.5°) with $\angle O_\mu O_A H_\mu$ = 21.0° and $\angle H_\mu O_A N_S$ = 28.8°. The subsequent IRC (intrinsic reaction coordinate) calculations with the TS2 structure as the starting point confirms that it is TS2 that is the transition state to connect the Int1 and Int2 intermediates (see Figure S2 in the SI). In addition, we could not obtain an intermediate with the O_AH group hydrogen bonding to the O_μ atom. Every attempt to locate this kind of minimum finally resulted in Int1 or Int2. This proton transfer turns out to be the rate-limiting step for hydrolysis, with a barrier of 19.8 kcal/mol (Figure 4) relative to the React species of Figure 2. The Int2 intermediate lies 18.6 kcal/mol higher than the reactant. The dispersion correction for TS2 looks very large (−11.0 kcal/mol) with React as the reference, but it considerably decreases to −0.4 kcal/mol if compared with Int1 (Figure 4). This means that the dispersion effect for this proton-transfer step is actually very small and that the big number of −11.0 kcal/mol derives from the accumulation from the first step of nucleophilic attack.

After Int2, there should be a transition state for the H_μ proton transfer from O_AH to N_S. However, all attempts to find this transition state failed and always led to an intermediate (Int3, Figure 3) with the H_μ proton bound at N_S. This can be attributed to a feature that the transition state is very early, which is speculated from a fact that Int3 is energetically much lower (4.1 kcal/mol) than Int2 (Figure 4). A further investigation by scanning the H_μ−N_S distance from 1.51 Å at Int2 to 1.06 Å at Int3 (see Figure S3 in the SI) shows that the guessed transition state is indeed extremely early with a very short O_A−H_μ distance (1.12 Å) that is rather close to that at Int2 (1.09 Å). Although the exact transition state for the proton transfer from O_AH to N_S could not be obtained, its energy is supposed to be lower than that of TS2 since the intermediate after it (i.e., Int3) is lower than the intermediate before TS2 (i.e., Int1) in energy (see Figure 4). Therefore, the failure in optimizing this transition state should not change the conclusion that the second step of proton transfer from $O_\mu H^-$ to Asp285 (O_A) is rate-limiting. In the Int3 intermediate, the distance between the H_μ proton and the N_S atom is 1.06 Å. As the nitrogen becomes protonated, the C_S−N_S bond for the peptide is elongated to 1.62 Å from 1.51 Å at Int2, implying that it is in principle ready to cleave.

3.2.3. C−N Bond Cleavage. From Int3, a transition state for the C_S−N_S peptide bond cleavage (TS3) and the resulting product (Prod) have been optimized and shown in Figure 3. The C_S−N_S distance is calculated to be 2.05 Å at TS3, which is finally elongated to 2.50 Å at Prod. TS3 has an imaginary frequency of 155*i* cm^{-1}, with a barrier of 15.4 kcal/mol compared with the reactant state of Figure 2 (see Figure 4). Prod is 12.1 kcal/mol higher than React in energy. When compared with Int3, the dispersion effects for the reaction barrier and energy of this step are computed to be small (0.7 and 1.7 kcal/mol, respectively). It is worth mentioning again that we did not consider the regeneration process after the C−N bond cleavage, which may involve the leaving of products and the rebridging between the two zinc ions by a hydroxide originated from a water molecule. To estimate the energy cost/gained during the substrate docking and the active-site regeneration, an uncatalyzed hydrolysis of *β*-aspartyl alanine in aqueous solution, where carboxylates and amidos are respectively presented as -COO^- and -NH_3^+, was calculated by the B3LYP/6-311+G(2d,2p) method with solvation (ε = 80) and dispersion (DFT-D3) effects included. The obtained reaction energy with ZPEs added is 7.6 kcal/mol, a number smaller than that in the IAD-catalyzed reaction (12.1 kcal/mol, Figure 4). The energy difference between them (−4.5 kcal/mol) may imply the energy gained during the substrate docking and the active-site regeneration which are not calculated in this study.

In summary, our calculations by approach II give a general support to the previously proposed mechanism.[49] The IAD reaction proceeds through a stepwise pathway, i.e., a nucleophilic attack on the peptide carbonyl carbon by the bridging hydroxide ($O_\mu H^-$) leading to a tetrahedral *gem*-diolate intermediate, two steps of proton transfer from $O_\mu H^-$ to Asp285 and subsequently to the nitrogen of the peptide bond, and the final cleavage of the C−N peptide bond. The rate-

DOI: 10.1021/acs.jctc.5b00246
J. Chem. Theory Comput. 2015, 11, 2525−2535

limiting step is found to be the proton transfer from $O_\mu H^-$ to Asp285, with an accumulated barrier of 19.8 kcal/mol (Figure 4). The main catalytic power originates from the Zn2 ion, which stabilizes the anionic tetrahedral intermediate. The first step of nucleophilic attack (from React to Int1 via TS1) was found to involve a large dispersion effect (about −10 kcal/mol). This big effect may derive from the significant approach of the substrate to the dizinc core. Apart from the initial step, dispersion effects are very small, for example, for the rate-limiting step of proton transfer from $O_\mu H^-$ to Asp285 (<1 kcal/mol). However, for this rate-limiting step, a dispersion effect accumulated from the first step is quite large (−11.0 kcal/mol), the ignoring of which would result in a too high barrier for the reaction, thereby leading to a completely different conclusion about the mechanism. It can thus be concluded that the inclusion of dispersion in quantum chemical modeling is of indispensability and significance for the interpretation of the IAD reaction mechanism.

3.3. Comparison with Approach I. The IAD reaction was also investigated using approach I, namely, geometry optimizations without dispersion followed by single-point calculations of dispersion effects. The mechanism calculated by approach I follows the same pattern as the case of approach II, and similar stationary points (Figure 5) and potential energy surface (Figure 6) have been obtained.

The overall geometrical parameters obtained by approach I (Figure 5) agree well with those by approach II (Figures 2 and 3), in particular for the strong interactions which reflect key chemistry. For example, in the enzyme−substrate complex ($React_{nd}$, Figure 5), the substrate is bound in the active site with a reasonable O_μ−C_S distance of 2.69 Å, a value that is very close to that at the React of Figure 2 (2.61 Å). From $React_{nd}$, a late transition state ($TS1_{nd}$, Figure 5) for the nucleophilic attack of $O_\mu H^-$ on the substrate was also found with an O_μ−C_S distance of 1.70 Å, in excellent agreement with the TS1 of Figure 3 (O_μ−C_S = 1.72 Å). With a tetrahedral *gem*-diolate intermediate ($Int1_{nd}$, Figure 5) formed in the first step of nucleophilic attack, the H_μ proton is transferred to the oxygen of Asp285 (O_A) via a transition state ($TS2_{nd}$, Figure 5) very similar to the TS2 of Figure 3, in which the O_AH group is also orientated inside the angle of $\angle O_\mu O_A N_S$ (48.8°) with $\angle O_\mu O_A H_\mu$ = 21.5° and $\angle H_\mu O_A N_S$ = 28.0°, to be compared to the angles of $\angle O_\mu O_A N_S$ = 49.5°, $\angle O_\mu O_A H_\mu$ = 21.0°, and $\angle H_\mu O_A N_S$ = 28.8° at the TS2 of Figure 3. This step results in a very unstable intermediate ($Int2_{nd}$, Figure 5), which is subsequently transformed into a new intermediate ($Int3_{nd}$, Figure 5) through another proton transfer from O_A to N_S. With the H_μ proton bound at the N_S atom, the $Int3_{nd}$ intermediate has a slightly longer C_S−N_S bond distance of 1.66 Å (C_S−N_S = 1.62 Å at the Int3 of Figure 3), implying that the C−N peptide bond becomes very weak. Finally, the C−N bond dissociates with C_S−N_S = 1.92 Å at the transition state ($TS3_{nd}$, Figure 5), leading to the two products of alanine and aspartic acid ($Prod_{nd}$, Figure 5). The $TS3_{nd}$ is calculated to have an imaginary frequency of 144*i* cm^{-1} which indicates a vibrational mode of the C_S−N_S bond dissociation. With the breaking of C−N bond, the C_S atom becomes sp^2-hybridized (a carboxylate) at $Prod_{nd}$ from sp^3-hybridized (tetrahedral geometry) at $Int3_{nd}$.

Approach I provides a potential energy surface (Figure 6) qualitatively consistent with the one by approach II (Figure 4), mainly in terms of the final energies. For all of the corresponding stationary points, the energy differences between the two surfaces are within 1.5 kcal/mol (see the black curves in Figures 4 and 6). In particular, using approach I, the second step of proton transfer from $O_\mu H^-$ to O_A is also predicted to be rate-limiting with an overall energy barrier of 20.0 kcal/mol, a number that is very close to the one obtained by approach II (19.8 kcal/mol, Figure 4). For this rate-limiting step, approach I also gives a small dispersion effect of −1.8 kcal/mol relative to $Int1_{nd}$ but a quite large effect of −7.1 kcal/mol accumulated from the reactant of $React_{nd}$. This again indicates that dispersion correction should be included in cluster modeling of the IAD reaction, at least in energy evaluation.

It is also noticed that, in the initial step of nucleophilic attack and the last step of alanine departure, there are a few discrepancies between the dispersion effects obtained by approach I and those by approach II. For example, approach I gives a dispersion effect of −5.3 kcal/mol for the first step (Figure 6), which is smaller than that predicted by approach II (−10.6 kcal/mol, Figure 4). For the last step, the dispersion effect is calculated to be 6.9 kcal/mol by approach I with $Int3_{nd}$ as the reference (Figure 6), while it is 1.7 kcal/mol by approach II with Int3 as the reference (Figure 4). The discrepancies of ∼5 kcal/mol mainly originate from the structural differences obtained by the two approaches. For example, The C_S−N_S distance (indicating the distance between the two products of alanine and aspartyl acid) is 2.73 Å at the $Prod_{nd}$ optimized by approach I (Figure 5), which is 0.23 Å shorter at the Prod by approach II (Figure 3). These differences render a few inconsistencies between approaches I and II. It has to be concluded that a qualitative consistency instead of complete consistency between approaches I and II was obtained mainly in the final energies and most key geometries.

The preceding results show a qualitative consistency between approaches I and II, not only in most key geometries but also in energetics, even if a quite big dispersion effect is indeed found in the present case of IAD. This not only demonstrates that both approaches are available for quantum chemical modeling of enzymatic reactions but also gives a strong indication that the results obtained by approach I (i.e., without dispersion included in geometry optimizations) in the previous studies of several systems[35,36,39−46] are convincing. With this, approach II is still suggested to be a preferential method since both geometry and energy are dispersion-corrected in that. On the other hand, it is conceivable that, if no remarkable dispersion effects are observed in the single-point calculations of dispersion on the basis of the geometries optimized without dispersion (i.e., by approach I), the inclusion of dispersion in geometry optimizations (i.e., the use of approach II) is unnecessary in quantum chemical modeling of enzymatic reactions.

3.4. Effects of Arg233. Using approaches I and II, the IAD reaction was also investigated based on a smaller chemical model of 147 atoms, which was obtained by removing the Arg233 residue from the model of Figure 2. The Arg233 is making two hydrogen bonds to one of oxygens of the alanine carboxylate and is positioned outside the alanine moiety of the dipeptide substrate (see Figure 2). Although it seems that the Arg233 only plays an assistant role in locating the substrate and shows little relevance to the chemistry in the reacting core, its exclusion from the model certainly results in a few interesting findings.

With Arg233 removed from the model, we also obtained a transition state for the first step of nucleophilic attack of $O_\mu H^-$ on the substrate (TS1-A in Figure S4 or $TS1\text{-}A_{nd}$ in Figure S5 in the SI) and a transition state for the second step of proton

DOI: 10.1021/acs.jctc.5b00246
J. Chem. Theory Comput. 2015, 11, 2525−2535

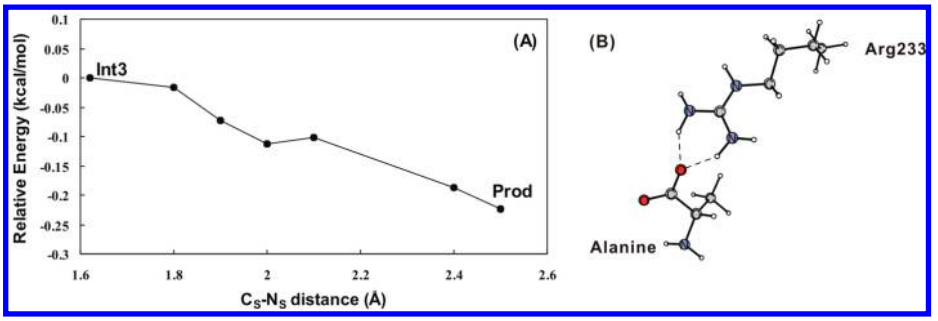

Figure 7. Dispersion effects between Arg233 and alanine (A) when the C_S−N_S distance is elongated from Int3 to Prod. The effects were calculated based on the geometries of Arg233 and alanine (B) extracted from the geometry optimizations of the chemical model of Figure 3.

transfer (TS2-A in SI Figure S4 or TS2-A_{nd} in SI Figure S5). However, the nature of the second transition state (TS2-A) was confirmed by IRC calculations (see Figure S6 in the SI) to connect a tetrahedral *gem*-diolate intermediate (Int1-A in SI Figure S4) and an intermediate with the H_μ proton bound at the nitrogen of peptide bond (Int3-A in SI Figure S4). This means that an intermediate with the H_μ proton bound at the Asp285 (such as Int2 in Figure 3) could not be found on the basis of this smaller model. In fact, we did not obtain this kind of intermediate though many attempts have been made, no matter which approach (approach I or II) was used. This can be rationalized by considering that the barrier for proton transfer from Asp285 to the nitrogen of the peptide bond (N_S) is tiny. Whenever a barrier is very small, it is possible to miss it depending on the chemical model and/or computational methods (for example, starting guess and convergence criteria). With this, it cannot be completely excluded that a barrier for proton transfer from $O_\mu H^-$ to the Asp285 oxygen (O_A) might also be missed by the previous calculations with Arg233 considered (in section 3.2.2), which led to two results mentioned earlier; i.e., (i) the nature of TS2 involves both proton transfer from $O_\mu H^-$ to O_A and the rotation of the O_AH group from O_μ to N_S to make a new hydrogen bond between O_AH and N_S, as well as (ii) an intermediate with the O_AH group hydrogen bonding to the O_μ atom could not be found. If this missing is true, the real nature of TS2 of Figure 3 would not involve the proton transfer from $O_\mu H^-$ to O_A but must only concern the rotation of the O_AH group from O_μ to N_S (i.e., the breaking of the hydrogen bond between O_AH and O_μ as well as the re-formation of a hydrogen bond between O_AH and N_S). Nevertheless, all things discussed in this paragraph do not change the conclusions about the mechanism, since the two barriers for proton transfer (from $O_\mu H^-$ to O_A and from O_AH to N_S) should be very small and thus would not significantly affect the overall barrier for the IAD reaction (see potential energy surfaces in SI Figures S7 and S8).

Once the H_μ proton is bound at the N_S atom (i.e., the Int3-A intermediate is formed), the C−N peptide bond should be broken to generate the products of alanine and aspartic acid. However, based on the smaller model without Arg233, we failed in optimizing the transition state for the C−N bond cleavage and the subsequent enzyme−product complex when dispersion was considered (namely, using approach II). The optimizations always came back to the Int3-A complex. To explain this confusion, an investigation was done by scanning the C_S−N_S distance from 1.59 Å at Int3-A to 3.00 Å (see Figure S9 in the SI). It shows that the complex energy continuously increases with the C_S−N_S distance elongated and no maximum appears. A further comparison with the case of the bigger model described earlier implies that this problem should result from the removal of Arg233 from the active-site model. Considering that the Arg233 side chain is placed outside the alanine moiety of the substrate (see Figure 2), the exclusion of Arg233 would result in the lack of attractive dispersion interaction between Arg233 and the alanine moiety, thus making the separation of alanine and aspartic acid to be a simple dissociation of a C−N single bond. Therefore, without the Arg233 residue, the elongation of C_S−N_S distance just costs energy. Meanwhile, using approach II and the bigger model with Arg233, a study by scanning the C−N distance from the Int3 structure of Figure 3 reveals that the attractive dispersion interaction between Arg233 and alanine increases with the C_S−N_S distance elongated (Figure 7). This clearly indicates that the Arg233 residue plays a role in facilitating the C−N bond cleavage and the departure of alanine product via the weak attractive dispersion interaction between them, although it seems to be unimportant for the chemistry. Of course, besides the attractive dispersion between Arg233 and alanine, other factors may also affect the departure of alanine, such as the hydrogen bonds between Arg233 and alanine as well as dispersion interactions between Arg233 and the groups other than alanine. Interestingly, when dispersion was not considered (i.e., using approach I), we succeeded in optimizing the transition state for the C−N bond cleavage (see TS3-A_{nd} in SI Figure S5) and the resultant enzyme−product complex (Prod-A_{nd} in SI Figure S5) on the basis of the smaller model without Arg233. This may attribute to a cancellation that the lack of attractive dispersion from Arg233 is compensated for by the exaggerated repulsion between alanine and aspartic acid. The latter is also derived from the ignoring of dispersion effects in approach I. In general, these results indicate that when dispersion is added in quantum chemical modeling of enzymatic reactions, particular carefulness should be paid to the steps involving group leaving, as well as group binding (for example, the initial step including substrate binding to the catalyst). At least, all residues surrounding the substrates and other concerned groups should be included in the chemical model, even if some of them appear to be of little relevance to the chemistry in the reacting core.

In summary, an inconsistency between approaches I and II was observed when a smaller model without Arg233 was employed. This along with the results based on the bigger model points out that the dispersion interactions lost with the removal of Arg233 are essentially responsible for determining equilibrium geometries. This indicates that the observation of inconsistency between approaches I and II in quantum chemical modeling most likely means the existence of important dispersion effects.

DOI: 10.1021/acs.jctc.5b00246
J. Chem. Theory Comput. 2015, 11, 2525−2535

4. CONCLUSIONS

In this work, we include dispersion in quantum chemical modeling of enzymatic reaction mechanisms by two different procedures, i.e., (i) geometry optimizations followed by single-point calculations of dispersion effects (referred to as approach I) and (ii) the inclusion of dispersion throughout geometry optimization and energy evaluation (approach II). As an example, the reaction mechanism of binuclear zinc isoaspartyl dipeptidase (IAD) was investigated respectively by approaches I and II, on the basis of a 169-atom chemical model built from the X-ray crystal structure. Transition states and intermediates along the reaction pathway were located and characterized, and potential energy surfaces obtained by approaches I and II were presented, respectively.

The calculations show a qualitative consistency between approaches I and II in energetics and most key geometries, even if a quite big dispersion effect is indeed observed in the present case of IAD. This not only demonstrates that both approaches are available for quantum chemical modeling of enzymatic reactions, but also gives strong support to the results obtained by approach I in the previous studies of metal-containing systems.[35,36,39−46] It is worth noting that approach II is still a preferential method since both geometry and energy are dispersion-corrected in that. Moreover, an inconsistency between approaches I and II was found when a smaller model without Arg233 (147 atoms) was employed. This indicates that the observation of inconsistent results between approaches I and II most likely implies the existence of important dispersion interactions which are essentially responsible for determining equilibrium geometries of a given system.

The calculations give a general support to the previous mechanism (Scheme 2)[49] and provide more details. The mechanistic characteristics of IAD concluded from the calculations are summarized as follows:

(1) The IAD reaction proceeds through a stepwise pathway, i.e., a nucleophilic attack on the peptide carbonyl carbon by the bridging hydroxide ($O_\mu H^-$) leading to a tetrahedral *gem*-diolate intermediate, two steps of proton transfer from $O_\mu H^-$ to Asp285 and subsequently to the nitrogen of peptide bond, and the final cleavage of the C−N peptide bond. The bridging hydroxide is demonstrated to be able to work as a nucleophile directly from its bridging position, similarly to previous calculations on other binuclear zinc enzymes, such as aminopeptidase from *Aeromonas proteolytica* (AAP),[69] phosphotriesterase (PTE),[28,70,71] and dihydroorotase (DHO).[72] The main catalytic power originates from the Zn2 ion, which stabilizes the developing charge of the anionic tetrahedral intermediate, thereby lowering the barrier of the nucleophilic attack.

(2) The rate-limiting step is found to be the second step of proton transfer from $O_\mu H^-$ to Asp285 (with an accumulated barrier of ∼20 kcal/mol). The initial nucleophilic attack by $O_\mu H^-$ is not rate-limiting, which was also observed in other binuclear zinc hydrolases (PTE, AAP, DHO, and glyoxalase II[73]).

(3) Apart from the initial step, dispersion effects are very small, for example, for the rate-limiting step of proton transfer from $O_\mu H^-$ to Asp285 (<1 kcal/mol). The dispersion effect in the first step of nucleophilic attack is calculated to be large (about −10 kcal/mol), because this step involves the substrate approaching the dizinc core. This big dispersion effect means that it is necessary and significant to include dispersion in cluster modeling of the IAD reaction.

(4) Arg233, a residue that is placed outside the alanine moiety of the substrate and making two hydrogen bonds to one of oxygens of the alanine carboxylate, plays an important role in assisting in the leaving of alanine product partially via the attractive dispersion interaction between them. The removal of Arg233 from the model would result in inconsistent results between approaches I and II. these results indicate that when dispersion is considered in quantum chemical modeling of enzymatic reactions, particular carefulness should be paid to the steps involving group leaving, as well as group binding (for example, the initial step involving substrate binding to the catalyst). At least, all residues surrounding the substrates and other concerned groups should be included in the chemical model, even if some of them appear to be of little relevance to the chemistry in the reacting core.

■ ASSOCIATED CONTENT

Supporting Information

Tables listing ZPE, solvation, and dispersion corrections and Cartesian coordinates of all optimized structures and figures showing ZPE corrections calculated by approaches I and II, schematic PESs, potential energy profiles, and optimized structures of stationary points along the reaction pathways calculated with approaches I and II. The Supporting Information is available free of charge on the ACS Publications website at DOI: 10.1021/acs.jctc.5b00246.

■ AUTHOR INFORMATION

Corresponding Author

*E-mail: shlchen@bit.edu.cn.

Funding

This work was financially supported by the Major State Basic Research Development Programs of China (Grant 2011CBA00701), the National Natural Science Foundation of China (Grant 21373027), the 111 Project (Grant B07012), and Beijing Nova Program (Grant Z151100000315055).

Notes

The authors declare no competing financial interest.

■ REFERENCES

(1) Blomberg, M. R. A.; Borowski, T.; Himo, F.; Liao, R.−Z.; Siegbahn, P. E. M. *Chem. Rev.* **2014**, *114*, 3601−3658.
(2) Siegbahn, P. E. M.; Blomberg, M. R. A. *Chem. Rev.* **2010**, *110*, 7040−7061.
(3) Siegbahn, P. E. M. *Q. Rev. Biophys.* **2003**, *36*, 91−145.
(4) Noodleman, L.; Lovell, T.; Han, W.−G.; Li, J.; Himo, F. *Chem. Rev.* **2004**, *104*, 459−508.
(5) Siegbahn, P. E. M.; Borowski, T. *Acc. Chem. Res.* **2006**, *39*, 729−738.
(6) Himo, F. *Theor. Chem. Acc.* **2006**, *116*, 232−240.
(7) Ertem, M. Z.; Cramer, C. J.; Himo, F.; Siegbahn, P. E. M. *J. Biol. Inorg. Chem.* **2012**, *17*, 687−698.
(8) Himo, F.; Siegbahn, P. E. M. *Chem. Rev.* **2003**, *103*, 2421−2456.
(9) Manta, B.; Raushel, F. M.; Himo, F. *J. Phys. Chem. B* **2014**, *118*, 5644−5652.
(10) Chen, S.−L.; Pelmenschikov, V.; Blomberg, M. R. A.; Siegbahn, P. E. M. *J. Am. Chem. Soc.* **2009**, *131*, 9912−9913.
(11) Leopoldini, M.; Russo, N.; Toscano, M. *J. Am. Chem. Soc.* **2007**, *129*, 7776−7784.
(12) Alberto, M. E.; Leopoldini, M.; Russo, N. *Inorg. Chem.* **2010**, *50*, 3394−3403.

DOI: 10.1021/acs.jctc.5b00246
J. Chem. Theory Comput. 2015, 11, 2525−2535

(13) Ribeiro, A. J. M.; Alberto, M. E.; Ramos, M. J.; Fernandes, P. A.; Russo, N. *Chem.—Eur. J.* **2013**, *19*, 14081−14089.
(14) Marino, T.; Russo, N.; Toscano, M. *Chem.—Eur. J.* **2013**, *19*, 2185−2192.
(15) Patton, G. C.; Stenmark, P.; Gollapalli, D. R.; Sevasti, R.; Kursula, P.; Flodin, S.; Schuler, H.; Swales, C. T.; Eklund, H.; Himo, F.; Nordlund, P.; Hedstrom, L. *Nat. Chem. Biol.* **2011**, *7*, 950−958.
(16) Leopoldini, M.; Russo, N.; Toscano, M.; Dulak, M.; Wesolowski, T. A. *Chem.—Eur. J.* **2006**, *12*, 2532−2541.
(17) Marino, T.; Russo, N.; Toscano, M. *J. Am. Chem. Soc.* **2005**, *127*, 4242−4253.
(18) Sousa, S. F.; Fernandes, P. A.; Ramos, M. J. *J. Am. Chem. Soc.* **2007**, *129*, 1378−1385.
(19) Cerqueira, N. M. F. S. A.; Fernandes, P. A.; Eriksson, L. A.; Ramos, M. J. *Biophys. J.* **2006**, *90*, 2109−2119.
(20) Liu, H.−N.; Robinet, J. J.; Ananvoranich, S.; Gauld, J. W. *J. Phys. Chem. B* **2007**, *111*, 439−445.
(21) Cho, K.-B.; Gauld, J. W. *J. Phys. Chem. B* **2005**, *109*, 23706−23714.
(22) Hopmann, K. H.; Hallberg, B. M.; Himo, F. *J. Am. Chem. Soc.* **2005**, *127*, 14339−14347.
(23) Das, B.; Daver, H.; Singh, A.; Singh, R.; Haukka, M.; Demeshko, S.; Meyer, F.; Lisensky, G.; Jarenmark, M.; Himo, F.; Nordlander, E. *Eur. J. Inorg. Chem.* **2014**, *13*, 2204−2212.
(24) Liao, R.-Z.; Yu, J.-G.; Himo, F. *J. Chem. Theory Comput.* **2011**, *7*, 1494−1501.
(25) Lind, M. E. S.; Himo, F. *Angew. Chem., Int. Ed.* **2013**, *52*, 4563−4567.
(26) Sevastik, R.; Himo, F. *Bioorg. Chem.* **2007**, *35*, 444−457.
(27) Hopmann, K. H.; Guo, J.-D.; Himo, F. *Inorg. Chem.* **2007**, *46*, 4850−4856.
(28) Chen, S.-L.; Fang, W.-H.; Himo, F. *Theor. Chem. Acc.* **2008**, *120*, 515−522.
(29) Becke, A. D. *J. Chem. Phys.* **1993**, *98*, 1372−1377.
(30) Becke, A. D. *J. Chem. Phys.* **1993**, *98*, 5648−5652.
(31) Lee, C.; Yang, W.; Parr, R. G. *Phys. Rev. B* **1988**, *37*, 785−789.
(32) Jensen, K. P.; Ryde, U. *J. Phys. Chem. A* **2003**, *107*, 7539−7545.
(33) Lewin, J. L.; Heppner, D. E.; Cramer, C. J. *J. Biol. Inorg. Chem.* **2007**, *12*, 1221−1234.
(34) Gherman, B. F.; Cramer, C. J. *Coord. Chem. Rev.* **2009**, *253*, 723−753.
(35) Siegbahn, P. E. M.; Blomberg, M. R. A.; Chen, S.-L. *J. Chem. Theory Comput.* **2010**, *6*, 2040−2044.
(36) Chen, S.-L.; Blomberg, M. R. A.; Siegbahn, P. E. M. *J. Phys. Chem. B* **2011**, *115*, 4066−4077.
(37) Grimme, S. *J. Comput. Chem.* **2004**, *25*, 1463−1473.
(38) Grimme, S. *J. Comput. Chem.* **2006**, *27*, 1787−1799.
(39) Liu, Y.-F.; Yu, J.-G.; Siegbahn, P. E. M.; Blomberg, M. R. A. *Chem.—Eur. J.* **2013**, *19*, 1942−1954.
(40) Hirao, H. *J. Phys. Chem. A* **2011**, *115*, 9308−9313.
(41) Chen, S.-L.; Blomberg, M. R. A.; Siegbahn, P. E. M. *Chem.—Eur. J.* **2012**, *18*, 6309−6315.
(42) Chen, S.-L.; Blomberg, M. R. A.; Siegbahn, P. E. M. *Phys. Chem. Chem. Phys.* **2014**, *16*, 14029−14035.
(43) Sun, S.; Li, Z.-S.; Chen, S.-L. *Dalton Trans.* **2014**, *43*, 973−981.
(44) Siegbahn, P. E. M.; Blomberg, M. R. A. *J. Chem. Theory Comput.* **2014**, *10*, 268−272.
(45) Efremenko, I.; Neumann, R. *J. Phys. Chem. A* **2011**, *115*, 4811−4826.
(46) Chen, F.; Li, X.; Wang, B.; Xu, T.; Chen, S.-L.; Liu, P.; Hu, C. *Chem.—Eur. J.* **2012**, *18*, 9870−9876.
(47) Haley, E. E. *J. Biol. Chem.* **1968**, *243*, 5748−5752.
(48) Thoden, J. B.; Marti-Arbona, R.; Raushel, F. M.; Holden, H. M. *Biochemistry* **2003**, *42*, 4874−4882.
(49) Martí-Arbona, R.; Fresquet, V.; Thoden, J. B.; Davis, M. L.; Holden, H. M.; Raushel, F. M. *Biochemistry* **2005**, *44*, 7115−7124.
(50) Kabsch, W. *J. Appl. Crystallogr.* **1988**, *21*, 916−924.
(51) Frisch, M. J.; Trucks, G. W.; Schlegel, H. B.; Scuseria, G. E.; Robb, M. A.; Cheeseman, J. R.; Scalmani, G.; Barone, V.; Mennucci, B.; Petersson, G. A.; Nakatsuji, H.; Caricato, M.; Li, X.; Hratchian, H. P.; Izmaylov, A. F.; Bloino, J.; Zheng, G.; Sonnenberg, J. L.; Hada, M.; Ehara, M.; Toyota, K.; Fukuda, R.; Hasegawa, J.; Ishida, M.; Nakajima, T.; Honda, Y.; Kitao, O.; Nakai, H.; Vreven, T.; Montgomery, J. A., Jr.; Peralta, J. E.; Ogliaro, F.; Bearpark, M.; Heyd, J. J.; Brothers, E.; Kudin, K. N.; Staroverov, V. N.; Kobayashi, R.; Normand, J.; Raghavachari, K.; Rendell, A.; Burant, J. C.; Iyengar, S. S.; Tomasi, J.; Cossi, M.; Rega, N.; Millam, J. M.; Klene, M.; Knox, J. E.; Cross, J. B.; Bakken, V.; Adamo, C.; Jaramillo, J.; Gomperts, R.; Stratmann, R. E.; Yazyev, O.; Austin, A. J.; Cammi, R.; Pomelli, C.; Ochterski, J. W.; Martin, R. L.; Morokuma, K.; Zakrzewski, V. G.; Voth, G. A.; Salvador, P.; Dannenberg, J. J.; Dapprich, S.; Daniels, A. D.; Farkas, O.; Foresman, J. B.; Ortiz, J. V.; Cioslowski, J.; Fox, D. J. *Gaussian 09*, Revision D.01; Gaussian: Wallingford, CT, USA, 2009.
(52) Klamt, A.; Schüürmann, G. *J. Chem. Soc., Perkin. Trans.* **1993**, *2*, 799−805.
(53) Cammi, R.; Mennucci, B.; Tomasi, J. *J. Phys. Chem. A* **1999**, *103*, 9100−9108.
(54) Barone, V.; Cossi, M. *J. Phys. Chem. A* **1998**, *102*, 1995−2001.
(55) Tomasi, J.; Mennucci, B.; Cammi, R. *Chem. Rev.* **2005**, *105*, 2999−3094.
(56) Siegbahn, P. E. M.; Blomberg, M. R. A. *Chem. Rev.* **2000**, *100*, 421−437.
(57) Yu, T.; Houk, K. N. *J. Chem. Theory Comput.* **2005**, *1*, 70−77.
(58) Grimme, S.; Antony, J.; Ehrlich, S.; Krieg, H. *J. Chem. Phys.* **2010**, *132*, No. 154104.
(59) Goerigk, L.; Grimme, S. *Phys. Chem. Chem. Phys.* **2011**, *13*, 6670−6688.
(60) Siegbahn, P. E. M. *J. Comput. Chem.* **2001**, *22*, 1634−1645.
(61) Sousa, S. F.; Fernandes, P. A.; Ramos, M. J. *J. Phys. Chem. A* **2007**, *111*, 10439−10452.
(62) Perdew, J. P.; Burke, K.; Ernzerhof, M. *Phys. Rev. Lett.* **1996**, *77*, 3865−3868.
(63) Perdew, J. P.; Burke, K.; Ernzerhof, M. *Phys. Rev. Lett.* **1997**, *78*, 1396.
(64) Adamo, C.; Barone, V. *J. Chem. Phys.* **1999**, *110*, 6158−6169.
(65) Becke, A. D. *J. Chem. Phys.* **1996**, *104*, No. 1040.
(66) Becke, A. D. *Phys. Rev. A* **1988**, *38*, 3098−3100.
(67) Zhao, Y.; Lynch, B. J.; Truhlar, D. G. *J. Phys. Chem. A* **2004**, *108*, 2715−2719.
(68) Chen, S.-L.; Li, Z.-S.; Fang, W.-H. *J. Inorg. Biochem.* **2012**, *111*, 70−79.
(69) Chen, S.-L.; Marino, T.; Fang, W.-H.; Russo, N.; Himo, F. *J. Phys. Chem. B* **2008**, *112*, 2494−2500.
(70) Kim, J.; Tsai, T.-C.; Chen, S.-L.; Himo, F.; Almo, S. C.; Raushel, F. M. *Biochemistry* **2008**, *47*, 9497−9504.
(71) Chen, S.-L.; Fang, W.-H.; Himo, F. *J. Phys. Chem. B* **2007**, *111*, 1253−1255.
(72) Liao, R.-Z.; Yu, J.-G.; Raushel, F. M.; Himo, F. *Chem.—Eur. J.* **2008**, *14*, 4287−4292.
(73) Chen, S.-L.; Fang, W.-H.; Himo, F. *J. Inorg. Biochem.* **2009**, *103*, 274−281.

DOI: 10.1021/acs.jctc.5b00246
J. Chem. Theory Comput. 2015, 11, 2525−2535